The influence of lipid type and peptide oligomerization on the transmembrane amyloid β-peptide: a simulation study

Chetan Poojari
Research Centre Jülich,
Institute of Complex Systems: Structural Biochemistry,
52425 Jülich, Germany

Andreas Kukol
University of Hertfordshire,
School of Life Sciences,
College Lane, Hatfield AL10 9AB, United Kingdom

Birgit Strodel[1]
Research Centre Jülich,
Institute of Complex Systems: Structural Biochemistry,
52425 Jülich, Germany

September 9, 2011

[1]Corresponding author. Address: Research Centre Jülich, Institute of Complex Systems: Structural Biochemistry, 52425 Jülich, Germany, Tel.: +49-2461-613670, Fax: +49-2461-618766

Abstract

The etiology of Alzheimer's disease is considered to be linked to interactions between amyloid-β (Aβ) and neural cell membranes causing membrane disruption and increased ion conductance. The effects of $A\beta$ on lipid behavior have been characterized experimentally, but structural and causal details are lacking. We have used atomistic molecular dynamics simulations totaling over 5 microseconds in simulation time to investigate the behavior of $A\beta_{42}$ in zwitterionic and anionic lipid bilayers. We considered transmembrane β-sheets (monomer and tetramer) resulting from a global optimization study and a helical structure obtained from an NMR study. In all simulations Aβ_{42} remained embedded in the bilayer, with slow unfolding of the peptide monomer in the bilayer occurring in some cases. The N-terminal segment of the peptide outside the membrane interacts strongly with the lipid headgroups, leading to a disordering of the headgroup arrangement. The most stable structure is the β-sheet tetramer due to interpeptide interactions. The transmembrane β-sheets allow the passage of water through the membranes, whereas helical Aβ_{42} facilitates this process only in the anionic bilayer. We dissect the influences of the lipid type on Aβ_{42} and the effects of Aβ_{42} on membrane integrity.

Key words: amyloid beta-peptide; phospholipid membranes; molecular simulations; protein-membrane interactions; Alzheimer's disease

Introduction

Alzheimer's disease (AD) is a neurodegenerative disorder associated with synaptic loss, abnormalities in functioning of neurons, neuronal cell death and extracellular accumulation of senile plaques composed of the neurotoxic amyloid-beta peptide (Aβ) (1, 2). Aβ is derived from the amyloid precursor protein (APP), a type-1 membrane integral glycoprotein through sequential cleavage by β- and γ-secretases (3). The major alloforms of Aβ are Aβ_{40} and Aβ_{42}, which differ by the presence of two amino acids, I41 and A42 at the C-terminus of the latter. The more hydrophobic Aβ_{42} is the prevalent alloform seen in amyloid plaques, and has a greater tendency to aggregate into fibrils and plaques (4, 5). There is acceptable evidence suggesting that Aβ exerts its cytotoxic effect by interacting with membranes of neurons and other cerebral cells, such as astrocytes, microglial and cerebral endothelial cells (6, 7). A potential pathway for Aβ toxicity lies in its ability to alter biophysical membrane properties (8–11). Aβ aggregates cause membrane disruption and increased permeability, allowing excessive leakage of ions, particularly calcium ions (12). This imbalance in calcium homeostasis promotes neuronal excitotoxicity (12, 13). Aβ_{42} oligomers interact with lipid raft related ganglioside GM1, further accelerating the amyloidogenic processing of APP (14).

Various experimental studies investigating the interactions between Aβ and phospholipids have revealed that Aβ prefers to bind to negatively charged lipids compared to zwitterionic lipids (15–17). It has been shown that the enhanced association of Aβ with anionic lipid membranes leads to the insertion of Aβ into the membrane (15–17) and induces the formation of β-sheets (15, 17–19) and Aβ fibrils(19–21). NMR spectroscopy studies on Aβ_{40} in a membrane-mimicking environment concluded that the peptide is unstructured in the N-terminal region from residues 1–14 and that the C-terminal hydrophobic residues from 15–36 adopt an α-helical conformation with a kink at residues 25-27 (22). This kink may be significant in membrane insertion and conformational rearrangements (22). Coles et al. proposed three possible models corresponding to different Aβ insertion depths in the membrane based on structural findings for Aβ_{40} (22). The two experimentally determined insertion depths have K28 and V24, respectively, at the membrane-water interface (22, 23). A third proposed model is with K16 at the membrane-water interface, where the entire α-helical conformation adopted by Aβ_{40} (residues 15-36) spans the plasma membrane (22). A study on soluble and

aggregated forms of Aβ_{40} on rat cortical synaptic plasma membrane using small angle X-ray diffraction and fluorescence spectroscopy showed that the monomer penetrates into the hydrophobic core of the bilayer, whereas the aggregated form was found interacting with the phospholipid headgroups (24). Similarly, soluble Aβ_{42} was found to intercalate the membrane of giant unilamellar vesicles composed of palmitoyl-oleoyl phosphatidylcholine (POPC) or POPC/sphingomyelin (SM)/cholesterol (Chol), altering permeability properties of the bilayer (25). However, permeabilization of lipid bilayers can also be caused by soluble amyloid oligomers (26). NMR, CD, fluorescence and monolayer studies on Aβ_{42} inserted into a POPC/POPS (palmitoyl-oleoyl phosphatidylserine) bilayer showed reduction in membrane stability with an increase in membrane fluidity (27). This study also indicated that Aβ_{42} alone could destabilize the membrane integrity in absence of ions, and that the peptide adopts a β-sheet structure in the membrane with increase in β content when Cu^{2+} is added (27). Further experimental work carried out on Aβ_{40} inserted into a zwitterionic phosphatidylcholine bilayer revealed that the perturbation of the bilayer integrity is caused by short β-sheet assemblies embedded in the lipid bilayer (28). Atomic force microscopy of Aβ_{42} (29) and Aβ_{40} (30) in reconstituted membranes revealed ion-channel-like structures, which are able to cause cellular ionic imbalance (30–34). Lal and coworkers also demonstrated through biochemical analysis that Aβ forms stable tetramers and hexamers in lipid membranes (29).

Various computational studies on Aβ interacting with lipids have been performed to gain structural information at an atomistic level (35–49). An atomistic model of Aβ channel structures developed by Nussinov and coworkers provided information about the Aβ conformation in membranes and ion-channel activity (35, 36). In another study they found that the channels break into mobile β-sheet subunits, which enable toxic ionic flux (37). Strodel and coworkers also proposed Aβ pore models composed of tetrameric to hexameric Aβ subunits, which are similar to the models suggested by Nussinov and coworkers (38). In (39) the stability of transmembrane β-barrel structures, each composed of eight Aβ fragments Aβ_{25-35}, was investigated. Molecular dynamics (MD) studies of Aβ_{40} inserted in a dipalmitoyl phosphatidylcholine (DPPC) bilayer with the peptide positioned with either K28, V24 or K16 at the membrane-water interface showed that in either case the peptide remained partially embedded in the membrane (40). Loss of α-helicity in favor of β-strands was observed when the peptide was inserted at K28 and V24, whereas with K16 at the interface α-helicity was retained.

For the deeper insertion depths, water molecules were seen entering the hydrophobic core accumulating near the charged residues of the peptide within the bilayer. It has also been reported that Aβ_{40} causes DPPC lipid headgroup disorder and reduces the membrane thickness around Aβ (41). In a recent study, Lemkul and Bevan explored the interactions between Aβ_{40} and several pure and mixed model membranes, and lipid rafts, both with and without GM1 (42). Aβ_{40} remained inserted in the membranes without GM1, but in several instances exited the raft containing GM1 initiated through hydrogen bonding of Aβ_{40} with GM1. MD simulations of Aβ_{42} with zwitterionic DPPC and anionic dioleoyl phosphatidylserine (DOPS) lipid membranes demonstrated the importance of charges on both bilayer surface and peptide for the adsorption of Aβ on the bilayer surface promoting Aβ aggregation and, as a consequence of interpeptide interactions coil-to-β conversion (43, 44). Another study on Aβ_{40} preinserted in a DPPC bilayer found the peptide exiting the membrane and adsorbing to its surface, with helix conformation being the major secondary structure observed in the membrane-adsorbed Aβ structure (46).

In the present MD study, we report the behavior of Aβ_{42} preinserted into zwitterionic (POPC and DPPC) and anionic (POPG) lipid bilayers. Due to conflicting experimental results as to whether Aβ is in a helical or in a β-sheet conformation in a lipid bilayer, we considered both transmembrane conformations as starting structures for our MD simulations. We used a β-sheet structure (monomer and tetramer) obtained from a global optimization approach (38) and a helix structure from an NMR study in an apolar solvent (22). During each of the 500 ns MD simulations, Aβ_{42} remains embedded in the lipid bilayer. We discuss our results in terms of structural stability of Aβ_{42} and its effects on membrane functionality.

Methods

Starting structures

The two initial Aβ_{42} structures are a β-sheet and a helical conformation. The transmembrane β-sheet was obtained from a study for the Aβ_{42} monomer and small oligomers using a global optimization approach in an implicit membrane model (38). The structure consists of an antiparallel β-sheet within the membrane with two turn regions (residues 23–29 and 37–38), and an N-

terminal β-hairpin outside the membrane. The more hydrophobic residues 17–42 are thus located within the membrane, whereas the more hydrophilic residues 1–16 occupy the extracellular space. We study this transmembrane β-sheet as monomer (denoted SHEET in the following) and tetramer as obtained in (38) [Fig. 1(a) and (b)]. The α-helical starting structure was obtained from an NMR study of $A\beta_{40}$ in an apolar solvent (PDB 1BA4) (22). We extended the 40 residue peptide to $A\beta_{42}$ by adding the two hydrophobic residues I41 and A42 in a coil conformation. Our motivation behind this extension was to study the role of the extra I41 and A42 residues in peptide-lipid interactions and the resulting structural changes in the peptide and membrane. Previous studies revealed an increased stability provided by I41 and A42 to the antiparallel β-sheet when compared to $A\beta_{40}$ (50). Furthermore, by using the same peptide we wanted to be able to compare our findings for the helical and β-sheet transmembrane structures. The helical structure was studied for two insertion depths: (i) with K16 (denoted HEL-16) and (ii) with D23 (denoted HEL-23) at the membrane-water interface [Fig. 1(c) and (d)]. All our simulations were carried out at the physiological charge of -3 for $A\beta_{42}$, modeling histidine residues uncharged. The N- and C-terminals were capped to nullify the effect of terminal residues in peptide-lipid interactions.

Molecular Dynamics Simulations

All MD simulations were performed with the GROMACS 4.0 package (51). The $A\beta_{42}$ peptide was described using the GROMOS96 53A6 force field (52), and the lipids were modeled with modified Berger force field parameters for use with the GROMOS96 53A6 force field (53). Details about the MD simulations can be found in the Supporting Material.

Analysis

The structural stability of $A\beta_{42}$ was analyzed separately for the N-terminal residues outside the membrane and the C-terminal residues inside the hydrophobic bilayer core. For $A\beta_{42}$ inserted at K16, the N-terminal residues thus range from 1–16 and the C-terminal residues from 17–42, whereas for $A\beta_{42}$ with D23 at the membrane-water interface residues 1–23 and residues 24–42 were considered as N- and C-terminal segment, respectively. The secondary structure of $A\beta_{42}$ was analyzed using the DSSP method (54). The probability of hydrogen bond (H-bond) formation between peptide and wa-

ter was considered based on a cutoff distance of 3.6 Å between donor and acceptor atoms and a cutoff angle off linearity of 30°. We used the grid-based membrane analysis tool GRIDMAT-MD to quantify the extent to which the peptide affects the lipid headgroup arrangement and bilayer thickness (55). For the bilayer thickness we report phosphate-to-phosphate (P–P) distances.

Results

The final structures after 500 ns of MD simulations of the SHEET, HEL-16, HEL-23 starting structures in a POPC, DPPC and a POPG bilayer are shown in Fig. 2. Here, the peptide residues rendered as pink spheres are those involved in H-bond formation with the water molecules entering the bilayer. In the Supporting Material the change of residual secondary structure during the MD simulations is presented (Figs. S1 and S2), as well as the mainchain root mean square deviation (RMSD) of the residues outside and inside the lipid bilayer (Figs. S3–S5). The RMSD by itself is not sufficient to decide upon the stability of $A\beta_{42}$ within the membrane since it contains the deviation from the starting structure in terms of secondary structure changes and overall rigid-body orientation of the peptide in the membrane. For instance, for the stable helical structure HEL-16 within POPC we obtain about the same RMSD as for the unstable HEL-16 in DPPC due to peptide tilt of the former. The peptide-lipid interaction energies, composed of electrostatic and van der Waals interactions, and averaged over the last 400 ns of the MD simulations are shown in Fig. S6.

The analysis of the bilayer properties is summarized in Table 1 and images of bilayer thickness calculated for the final states of the MD simulations are shown in Figs. S7 and S8. In all cases we observed a decreased area per lipid headgroup in the upper leaflet compared to the lower leaflet, and in comparison to the experimental and simulation values for the bilayers without peptide. This area contraction results from attractive electrostatic forces between $A\beta_{42}$ residues and lipid headgroups. For the bilayer thickness we find that the average thickness of POPC and POPG bilayers is hardly affected by embedded $A\beta_{42}$ with thickness changes less than 1 Å. However, Fig. S7 reveals that the POPC, POPG and DPPC thicknesses around $A\beta_{42}$ are decreased in order to improve the hydrophobic matching between bilayer and $A\beta_{42}$, whose hydrophobic width is smaller than those of the lipids. The three bilayers studied exhibit a similar thickness of about 2.5–3.0 nm in the

neighborhood of the peptide, which corresponds to the hydrophobic width of the latter for both β-sheet and helical structures. This implies that the decreased thinner region close to Aβ_{42} is compensated with an increase of the thickness further away from the peptide (56) as evidenced by Figs. S7 and S8. This effect is most pronounced for DPPC, for which we observe an increase of the average thickness by 3–4.5 Å compared to the pure bilayer, with values for the P–P distances reaching up to 5 Å (Fig. S7).

The transmembrane β-sheet

The β-sheet remained embedded in the membrane for all three bilayer types with minor loss of β-strands observed in the hydrophobic core of the bilayer (Figs. 2 and S1). The N-terminal segment of the peptide is adsorbed to the bilayer surface of the upper leaflet due to strong electrostatic interactions and hydrogen bonding. These interactions rupture the lipid packing and lead to a tilt of the lipids around the peptide, allowing passage of water molecules into the hydrophobic core of the bilayer. The lipid headgroups of the lower leaflet are shifted upwards into the hydrophobic core resulting from interactions with the negatively charged residues E22 and D23, thereby facilitating the entry of water molecules from the bottom of the bilayer. Most of these water molecules remain in the vicinity of the charged Aβ_{42} residues within the membrane. However, some of the water molecules are able to translocate the membrane, which is independent of the lipid type and can be attributed to non-hydrogen-bonded carbonyl and amide groups at the edges of the β-sheet. These peptide groups can thus form hydrogen bonds with the water molecules entering the lipid bilayer. Therefore, many hydrophobic residues are involved in peptide-water interactions in the hydrophobic bilayer core (Fig. 2). We find the β-sheet to be most stable in POPC and least stable in DPPC. In the DPPC simulation the salt bridge between D23 and K28, which stabilizes the turn between residues 23 and 29 (35), became broken. Instead, E22 and D23 interact with the headgroups of the lower leaflet leading to further destabilization of the peptide. In DPPC the peptide unfolds from β-sheet to coil and bend structures within the membrane except for residues L17–F20, L34–V36, V40 and I41, which remain in the β-state. These structural instabilities increase the influx of water molecules into the membrane core. In the simulation with POPG we observe a transient loss of β-sheet to coil from residues L17 to A21, and from sheet-turn-sheet to sheet-bend-coil for residues G33 to I41 during the initial 170 ns of the MD run. However, for the

remainder of the MD simulation the β-sheet has reformed and is considerably stable.

Helical Aβ_{42} with K16 at the membrane-water interface

The simulations of HEL-16 were performed for comparison with the β-sheet structure, which has K16 at the membrane-water interface. Like the β-sheet, the helical peptide did not exit the bilayer during any of the 500 ns MD simulations, and the N-terminal segment of the peptide associates with the bilayer surface (Fig. 2). A key finding of the simulations with POPC and POPG is that the peptide moves upwards due to interactions between the the charged residues E22 and D23 and the headgroups of the upper leaflet lipids, so that these two residues leave the hydrophobic core and align with the bilayer-water interface, i.e., HEL-16 becomes HEL-23. These interactions cause a disordering of the upper leaflet around the peptide, allowing leakage of water molecules into the hydrophobic core of the bilayer. In the POPC bilayer, water molecules entering the upper leaflet mainly interact with residues E22–S26 around the headgroup region, whereas water molecules entering the lower leaflet interact with the C-terminal residues G37–A42. However, no passage of water molecules through the POPC membrane is observed for HEL-16, which is tilted within this bilayer. Conversion of the α-helix to turn structure is found for residues D23–S26, which are inside the membrane in the vicinity of the headgroup region interacting with water. A high stability of the transmembrane helical structure is seen for residues N27–V39, which are well placed within the hydrophobic core. The last three residues V40–A42 retained their coil structure and caused the lower lipid headgroups to slightly shift upwards. In POPG only residues K28–G37 of HEL-16 remain α-helical (i.e., the helix in POPG is less stable than in POPC), while the other residues adopt coil and turn conformations. Unlike in the POPC simulation, the helical Aβ_{42} is not tilted in the membrane core and allows water molecules to translocate the membrane, mediated via H-bonds between water and peptide.

In case of HEL-16 in a DPPC bilayer, the α-helical structure is only stable between residues A21 and A30, whereas the other residues inside the DPPC membrane (K16–F20 and I31–A42) unfold to turn and bend structures. A considerable amount of water molecules is able to enter the hydrophobic bilayer region (Table 1). However, the water molecules remain in the vicinity of the headgroup regions and mainly interact with residues V18–D23 and

G37–A42 as is the case for POPC. Therefore, no passage of water through the membrane was observed for the DPPC bilayer though the average number of H-bonds between water and peptide in the bilayer is of similar size as for SHEET in DPPC. Unlike HEL-16 in POPC and POPG, HEL-16 in DPPC does not move upwards leaving E22 and D23 inside the hydrophobic core, which induces helix-to-coil transitions in Aβ_{42}.

Helical Aβ_{42} with D23 at the membrane-water interface

HEL-23, like HEL-16, remained embedded in the membrane as stable α-helix (Fig. 2) in all three bilayers. Residues outside the membrane loose their helicity to disordered coil and turn conformations. Residues E22 and D23 interact strongly with the headgroups of the upper leaflet, causing headgroup disorder and a reduction of the area per lipid. Peptide tilt with respect to the bilayer normal is observed in POPC and DPPC bilayers, but not in POPG. In POPC, the helix is stable within the membrane between residues V24–V39. Water molecules interact with the peptide around the headgroup region, but there are no water molecules deep into the hydrophobic core. The comparison between HEL-16 and HEL-23 in POPC shows that both systems are very similar after 250 ns, when HEL-16 has moved upwards so that E22/D23 are at the membrane-water interface. In the simulation with DPPC, HEL-23 retains its transmembrane α-helical structure, what is different to HEL-16 in DPPC, which was not stable. Even the terminal hydrophobic residues I41 and A42 fold from coil to α-helix in HEL-23, adding further to the stability of this structure. The lipids around HEL-23 in the lower leaflet are shifted upwards to fill the space created by peptide disordering of the lipids in the upper leaflet, and to compensate for hydrophobic mismatch. As for POPC, there is no passage of water molecules through the bilayer. Simulations of HEL-23 in POPG revealed a loss of the α-helix from residues L17 to N27, which instead adopt coil and turn conformations. On the investigated timescale the α-helix is stable between residues K28 and G38. The last three residues extend to a coil structure reaching the bottom membrane surface, thereby disordering this headgroup region more pronounced as SHEET and HEL-16 in POPG. HEL-16 and HEL-23 in POPG are similar, like in POPC, after HEL-16 has moved upwards becoming HEL-23. HEL-23 facilitates the translocation of water molecules in the POPG bilayer.

Mixed POPC/POPG bilayer simulations of HEL-23

To shed more light on what is causing the differences of HEL-23 in POPC and POPG (i.e., this includes HEL-16 since it becomes HEL-23 in POPC and POPG), we performed two more 100 ns MD simulations of HEL-23 in mixed POPC/POPG bilayers with asymmetric lipid distribution. In one simulation the upper leaflet was composed of POPG lipids and the lower leaflet of POPC lipids, while in the other simulation it was the other way round, i.e., POPC in the upper and POPG in the lower leaflet. The helical structure was preinserted with D23 at the membrane-water interface (HEL-23). The final structures after 100 ns of MD simulations are shown in Fig. 3. In either case, $A\beta_{42}$ is tilted unlike the helical structure in a POPG only membrane. We therefore conclude that the straight alignment of HEL-23 in POPG must be due to the interaction between the α-helical dipole moment with the dipole potential of the anionic POPG bilayer, which in turn allows the passage of water through the membrane in the POPG only simulations. In the mixed POPC/POPG bilayer simulations we only observe translocation of water molecules when POPC is in the upper and POPG in the lower leaflet.

Furthermore, the comparison of the POPC/POPG and POPG/POPC (here the order of the lipids refers to the upper and lower leaflet) results demonstrates a destabilizing effect of the anionic POPG headgroups in the upper leaflet on the helical structure up to residue 26 [Fig. 3(a)]. In this region the helical structure is lost in favor of coil structures due to interactions between the polar peptide residues and the anionic headgroups. This is not the case when POPC is in the upper leaflet, where the helix is stable from residue 15 onwards. Between residues 22 and 36 the helix is stable in both POPC/POPG and POPG/POPC bilayers, i.e., these transmembrane residues are not or only mildly influenced by the type of the headgroups in both leaflets. In this region the type of the lipid tails, which is the same for POPC and POPG, is the determining factor for the stability of the transmembrane $A\beta_{42}$ helix. Residues 37 to 42 are in different coil conformations in the POPC/POPG and POPG/POPC simulation. For the POPC/POPG simulation the C-terminus of $A\beta_{42}$ is closer to the lower membrane surface than when POPC is in the bottom leaflet. This finding agrees with the results for POPC and POPG only simulations (Fig. 2), and adds further to the leakage of water into the hydrophobic core in case that POPG is in the lower leaflet.

The transmembrane β-sheet tetramer

Our motivation for studying the transmembrane β-sheet tetramer was to test whether it is more stable than the single transmembrane β-sheet and could thus serve as building block for a pore composed of several Aβ_{42} β-sheet oligomers (35–38). Furthermore, we wanted to investigate whether the Aβ_{42} tetramer is able to disturb the lipid bilayer sufficiently in order to allow water and ion passage through the membrane. The final structure of this 500 ns MD simulation in a POPC bilayer is shown in Fig. 4. We observe that unlike in the monomeric SHEET the N-terminal β-hairpins are stable in the tetramer. They rather interact with each other than with the bilayer surface, causing the N-terminal regions to stick out into the water instead of being adsorbed to the bilayer surface as we observed for all monomeric transmembrane Aβ_{42} structures. Along with the charged and polar residues in the N-terminal half of the peptide this structure might thus act as a funnel for ions to be inserted into the membrane in larger Aβ assemblies composed of our tetramer model (57). The transmembrane β-strands were more stable throughout the simulations compared to the β-sheet monomer. This increased stability is due to favorable interpeptide interactions (38), including H-bonds between β-strands (backbone H-bonds) and intermolecular salt bridges between D23 and K28. This increase in peptide-peptide interactions leads to a decrease in peptide-lipid interactions as Fig. S6 supports. Water molecules enter the membrane in the upper and lower leaflet and mainly interact with the negatively charged residues E22 and D23 around the lower lipid headgroup region and with polar residues near the upper headgroup region. However, water can pass through the membrane via the outside edges of the β-sheets due to carbonyl and amide groups, which do not form inter- or intrapeptide H-bonds. Table 1 shows that, on average, there are 95 H-bonds between Aβ_{42} and water within the membrane, i.e., around 24 H-bonds per peptide. The tetramer thus leads to an increased bilayer permeability compared to the β-sheet monomer.

Discussion

In all cases Aβ_{42} remained inside the bilayer throughout the MD simulations on the sub-microsecond scale. This finding is independent of the secondary structure of the starting conformation and the lipid bilayer type, and agrees

well with experimental findings for soluble Aβ, which was reported to intercalate deeply into the plasma membrane hydrocarbon core (24).

Aβ_{42} in palmitoyl-oleoyl bilayers (POPC and POPG)

The behavior of Aβ_{42} in POPC and POPG bilayers is quite similar, yet different from when the peptide is inserted in a DPPC bilayer. This observation leads to the conclusion that once the peptide has entered the membrane, its structural stability and effects on the membrane are mainly influenced by the lipid tails and not so much by the type of head groups. Here, important aspects are the length of the hydrophobic tails in terms of hydrophobic mismatch and saturation of the lipid tails, which is in agreement with findings of Lemkul and Bevan (42). The anionic headgroup charges of POPG induce structural transformations to coil conformations in the Aβ_{42} residues close to the headgroup regions. Aβ_{42} inserted into a POPC bilayer as a β-sheet or helix is relatively stable within the membrane core, which is supported by experimental results stating that Aβ_{42} peptide remains well embedded in the lipid environment composed of POPC or POPC/SM/Chol altering cohesion between the membrane components and membrane permeability (25). The stable β structure seen in our simulations is also in agreement with experimental work showing that Aβ_{40} is present as a β-sheet in a POPC bilayer (28). Another study reported β content also for Aβ_{42} in the membrane hydrophobic core, and demonstrated that the incorporation of Aβ_{42} into a POPC/POPS mixed bilayer destabilizes the membrane increasing its permeability properties (27). We observed an increased bilayer permeability for the β-sheet compared to the helical Aβ_{42} structures. The largest number of water molecules passing the POPC bilayer is seen for the β-sheet tetramer, which is at the same time also the most stable transmembrane Aβ_{42} structure in our study. This is in agreement to experimental work reporting that Aβ_{42} forms stable tetramers within membranes (29), and that Aβ oligomers cause membrane permeabilization (26).

Helical Aβ_{42} was also considerably stable during our MD simulations. The HEL-16 conformation, however, moved upwards in both POPC and POPG so that residues E22 and D23 can leave the hydrophobic core reaching the membrane-water interface. The headgroup type influences the orientation of helical Aβ_{42} in the bilayer, leading to a tilt of the peptide in POPC and a straight alignment in POPG, and the translocation of water molecules, which is possible in POPG but not in POPC. Determining factors for the rigid-body

orientation of transmembrane proteins (or parts of it) relative to the bilayer normal are usually hydrophobic matching and packing of lipid chains around the protein (56). The former is especially important in lipid bilayers with a thickness shorter than the hydrophobic width of the protein. However, this does not apply to the Aβ_{42} structures under study as their hydrophobic widths are by 5–10 Å shorter than the bilayer thicknesses. Instead the anionic surface charge of POPG was found to inhibit the tilt of helical Aβ_{42} by interacting with the helical dipole moment of Aβ_{42}.

Aβ_{42} in DPPC bilayers

The simulations with DPPC resulted in a more pronounced loss of secondary structure for both SHEET and HEL-16 conformations within the membrane core as compared to the corresponding POPC and POPG simulations. These structural instabilities can be attributed to hydrophobic mismatch as the DPPC bilayer is generally more ordered than the unsaturated lipids in POPC and POPG bilayers. Lipid order leads to a larger bilayer thickness (Table 1), giving rise to an increased hydrophobic mismatch between Aβ_{42} and DPPC. An increased hydrophobic mismatch, in turn, inflicts an ordering effect on the lipid bilayer (56). This effect can be observed in the increased bilayer thicknesses further away from Aβ_{42}, which is especially pronounced in DPPC since saturated acyl chains exhibit poorer adaptation to the peptide than lipids with unsaturated chains (56). The higher simulation temperature in the MD simulations with DPPC may also add to more fluctuations in the peptide. The HEL-23 conformation, however, adopts a stable α-helix inside the membrane.

Our findings for the helical structures inserted in a DPPC bilayer are different to those obtained from MD simulations by Xu et al. (46). They inserted the helical structure with K28 at the DPPC membrane-water interface and observed Aβ_{40} to leave the hydrophobic core in less than 100 ns associating with the bilayer surface, where it remained α-helical. These discrepancies may be due to (i) the missing two hydrophobic residues I41 and A42 in Aβ_{40}, (ii) the different initial insertion depths, (iii) usage of different force fields, and (iv) different protocols employed to insert the peptide into the membrane (40). Other MD simulations with Aβ_{40} in a DPPC bilayer reported the peptide to remain partially embedded in the bilayer, when it was inserted with K28 at the membrane-water interface (40). However, a complete loss of helicity was observed within the first 10 ns of these sim-

ulations. When Aβ_{40} was inserted with K16 at the interface, the peptide remained embedded in the bilayer and retained its α-helicity in the central segment (40), which is in agreement with our results.

Water permeation

Strong interactions between the Aβ_{42} peptide and lipids give rise to a disordering of the lipid headgroup arrangement and a tilt of the lipids around the peptide, allowing entry of water molecules into the hydrophobic membrane core, where they can form H-bonds with polar and non-polar Aβ_{42} residues. For water translocation due to transmembrane Aβ_{42} to take place, we could identify following cases: (i) The β-sheet conformation always allows the passage of water molecules, enabled via H-bonds of the water molecules with peptide carbonyl and amide groups not involved in intra- or interpeptide (the latter only in the case of the tetramer) H-bonds. This behavior is independent of the type of the lipid headgroup and the lipid tail. (ii) In case of the helix, where all peptide carbonyl and amide groups form intrapeptide H-bonds, the water passage is hampered as our results for the helical structures in POPC and DPPC evidence. However, for the POPG bilayer we did observe transmembrane water passage, which is accompanied by a partial transformation of the helix into coil conformations since the stabilizing intrapeptide H-bonds are temporarily replaced by H-bonds with water molecules. (iii) Furthermore, the helical structures in POPG are not tilted, whereas the most tilted helices in POPC and DPPC (HEL-23 only) block the water molecules from entering deep into the hydrophobic membrane core. Thus, the peptide tilt plays a role in hindering transmembrane water flow. (iv) In case of the helix the anionic membrane surface of POPG is also important for mediating the entrance of water molecules into the hydrophobic core as the mixed POPC/POPG simulations revealed (Fig. 3). Here, water could only pass the membrane if POPG is in the lower bilayer. The entry of water molecules in the upper bilayer is mainly caused by the charged residues E22, D23 and K28, and not so much by the headgroup type. (v) The more unstable the monomeric helix or β-sheet is (i.e., the more residues adopt a coil conformation and thus are not involved in intrapeptide H-bonds), the more water molecules can enter the hydrophobic membrane core. This finding can be observed, e.g., for the β-sheet in DPPC (Table 1). (vi) The highest permeability is observed for the β-sheet tetramer.

The presence of water molecules in the lipid bilayer due to inserted Aβ_{42}

was also observed in simulations of Lemkul et al. (40). During our simulations none of the Na^+ and Cl^- ions entered the hydrophobic membrane core. We found Na^+ ions being trapped around the lipid headgroups region, which is in line with findings for cell plasma membranes (58). The Na^+ ions near the upper leaflet also compensate the negative charge of -3 of $A\beta_{42}$. We conclude that probably larger transmembrane $A\beta$ assemblies are needed to enable transmembrane ion flow as observed experimentally (30–34).

Conclusions

Association of $A\beta$ with neuronal cell membranes and resulting neuronal toxicity is a well known AD hypothesis (59) with $A\beta$ exerting its cytotoxic effect by increasing membrane fluidity (24). Previously, it was reported that permeabilization of membranes was caused by $A\beta$ oligomers (26), but later it was shown that the $A\beta_{42}$ monomer can also intercalate the membrane and alter its properties (25). There is increasing evidence that $A\beta$ adopts a β conformation in the membrane (27, 28), yet an experimental atomistic model of membrane-bound $A\beta$ is still lacking. Molecular simulations offer the potential of predicting such structures (38, 57, 60), and, furthermore, provide information about how $A\beta$ fluctuates and interacts with lipid bilayers. To this end we performed molecular simulations of transmembrane $A\beta_{42}$ considering both helical and β-sheet conformations preinserted in POPC, DPPC and POPG bilayers. The MD simulations on the sub-microsecond timescale revealed the highest stability in POPC for both helical and β-sheet $A\beta_{42}$. Hydrophobic mismatch and lipid order of DPPC, and anionic surface charges of POPG bilayers are responsible for structural instabilities of $A\beta_{42}$ in these bilayers. However, $A\beta_{42}$ remained embedded in the bilayers in all of our MD simulations. The β-sheet is able to translocate water in all three bilayer types, whereas the helical structure can facilitate this process only in POPG. Comparing the stability of the α-helical and β-sheet structures, we find that the β-sheet is slightly more stable within the membrane. Its stability and ability to translocate water can be further increased via oligomerization, where favorable interpeptide interactions add to the stability of this structure (38). Membrane permeabilization by membrane-bound $A\beta$ is commonly observed experimentally (12, 26, 27). From these findings we conclude that $A\beta_{42}$ adopts a β-sheet conformation in the membrane, which is in agreement with experiment (15, 17–19, 27, 28). Possible structural models for the β-sheet monomer and tetramer are shown in Fig. 1.

Supporting references

Reference (61) appears in the Supporting Material.

Acknowledgments

References

1. Selkoe, D. J., 2000. The origins of Alzheimer disease - A is for amyloid. *J. Am. Med. Assoc.* 283:1615–1617.

2. Roberson, E. D., and L. Mucke, 2006. 100 years and counting: Prospects for defeating Alzheimer's disease. *Science* 314:781–784.

3. Thinakaran, G., and E. H. Koo, 2008. Amyloid Precursor Protein Trafficking, Processing, and Function. *J. Biol. Chem.* 283:29615–29619.

4. Jarrett, J. T., E. P. Berger, and P. T. Lansbury, 1993. The carboxy terminus of the beta-amyloid protein is critical for the seeding of amyloid formation - implications for the pathogenesis of Alzheimers-disease. *Biochemistry* 32:4693–4697.

5. Younkin, S. G., 1998. The role of A beta 42 in Alzheimer's disease. *J. Physiol. Paris* 92:289–292.

6. Mohamed, A., and E. P. de Chaves, 2011. A internalization by neurons and glia. *Int. J. Alzheimers Dis.* 2011:127984.

7. Williams, T. L., and L. C. Serpell, 2011. Membrane and surface interactions of Alzheimers $A\beta$ peptide – insights into the mechanism of cytotoxicity. *FEBS J.* 278:17.

8. Friedman, R., R. Pellarin, and A. Caflisch, 2009. Amyloid Aggregation on Lipid Bilayers and Its Impact on Membrane Permeability. *J. Mol. Biol.* 387:407–415.

9. Terzi, E., G. Holzemann, and J. Seelig, 1997. Interaction of Alzheimer beta-amyloid peptide(1-40) with lipid membranes. *Biochemistry* 36:14845–14852.

10. Buchsteiner, A., T. Hauss, S. Dante, and N. A. Dencher, 2010. Alzheimer's disease amyloid-beta peptide analogue alters the ps-dynamics of phospholipid membranes. *Biochim. Biophys. Acta-Biomembr.* 1798:1969–1976.

11. Eckert, G. P., W. G. Wood, and W. E. Mueller, 2010. Lipid Membranes and beta-Amyloid: A Harmful Connection. *Curr. Protein Pept. Sci.* 11:319–325.

12. Sepulveda, F. J., J. Parodi, R. W. Peoples, C. Opazo, and L. G. Aguayo, 2010. Synaptotoxicity of Alzheimer beta amyloid can be explained by its membrane perforating property. *PLoS One* 5.

13. Mattson, M. P., B. Cheng, D. Davis, K. Bryant, I. Lieberburg, and R. E. Rydel, 1992. Beta-amyloid peptides destabilize calicum homeostasis and render human cortical-neurons vulnerable to excitotoxicity. *J. Neurosci.* 12:376–389.

14. Peters, I., U. Igbavboa, T. Schuett, S. Haidari, U. Hartig, X. Rosello, S. Boettner, E. Copanaki, T. Deller, D. Koegel, W. G. Wood, W. E. Mueller, and G. P. Eckert, 2009. The interaction of beta-amyloid protein with cellular membranes stimulates its own production. *Biochim. Biophys. Acta-Biomembr.* 1788:964–972.

15. Terzi, E., G. Hölzemann, and J. Seelig, 1997. Interaction of Alzheimer -amyloid peptide(1-40) with lipid membranes. *Biochemistry* 36:14845–14852.

16. Ege, C., and K. Lee, 2004. Insertion of Alzheimer's Abeta 40 peptide into lipid monolayers. *Biophys. J.* 87:1732–1740.

17. Terzi, E., G. Holzemann, and J. Seelig, 1994. Alzheimer beta-amyloid peptide 25-35: electrostatic interactions with phospholipid membranes. *Biochemistry* 33:7434–7441.

18. McLaurin, J., and A. Chakrabartty, 1997. Characterization of the interactions of Alzheimer -amyloid peptides with phospholipid membranes. *Eur. J. Biochem.* 245:355–363.

19. Ege, C., J. Majewski, G. Wu, K. Kjaer, and K. Lee, 2005. Templating effect of lipid membranes on Alzheimer's amyloid beta peptide. *Chem. Phys. Chem.* 6:226–229.

20. Chauhan, A., I. Ray, and V. Chauhan, 2000. Interaction of amyloid beta-protein with anionic phospholipids: possible involvement of Lys28 and C-terminus aliphatic amino acids. *Neurochem. Res.* 25:423–429.

21. Chi, E. Y., C. Ege, A. Winans, J. Majewski, G. Wu, K. Kjaer, and K. Y. C. Lee, 2008. Lipid membrane templates the ordering and induces the fibrillogenesis of Alzheimer's disease amyloid- peptide. *Proteins: Struct., Func. and Bioinf.* 72:1–24.

22. Coles, M., W. Bicknell, A. A. Watson, D. P. Fairlie, and D. J. Craik, 1998. Solution structure of amyloid beta-peptide(1-40) in a water-micelle environment. Is the membrane-spanning domain where we think it is? *Biochemistry* 37:11064–11077.

23. Tischer, E., and B. Cordell, 1996. beta-amyloid precursor protein - Location of transmembrane domain and specificity of gamma-secretase cleavage. *J. Biol. Chem.* 271:21914–21919.

24. Mason, R. P., R. F. Jacob, M. F. Walter, P. E. Mason, N. A. Avdulov, S. V. Chochina, U. Igbavboa, and W. G. Wood, 1999. Distribution and fluidizing action of soluble and aggregated amyloid beta-peptide in rat synaptic plasma membranes. *J. Biol. Chem.* 274:18801–18807.

25. Ambroggio, E. E., D. H. Kim, F. Separovic, C. J. Barrow, C. J. Barrow, K. J. Barnham, L. A. Bagatolli, and G. D. Fidelio, 2005. Surface behavior and lipid interaction of Alzheimer beta-amyloid peptide 1-42: A membrane-disrupting peptide. *Biophys. J.* 88:2706–2713.

26. Kayed, R., Y. Sokolov, B. Edmonds, T. M. McIntire, S. C. Milton, J. E. Hall, and C. G. Glabe, 2004. Permeabilization of lipid bilayers is a common conformation-dependent activity of soluble amyloid oligomers in protein misfolding diseases. *J. Biol. Chem.* 279:46363–46366.

27. Lau, T. L., E. E. Ambroggio, D. J. Tew, R. Cappai, C. L. Masters, G. D. Fidelio, K. J. Barnham, and F. Separovic, 2006. Amyloid-beta peptide disruption of lipid membranes and the effect of metal ions. *J. Mol. Biol.* 356:759–770.

28. de Planque, M. R. R., V. Raussens, S. A. Contera, D. T. S. Rijkers, R. M. J. Liskamp, J. M. Ruysschaert, J. F. Ryan, F. Separovic, and A. Watts, 2007. β-sheet structured beta-amyloid(1-40) perturbs phosphatidylcholine model membranes. *J. Mol. Biol.* 368:982–997.

29. Lin, H., R. Bhatia, and R. Lal, 2001. Amyloid β protein forms ion channels: implications for Alzheimers disease pathophysiology. *FASEB J.* 15:2433–2444.

30. Quist, A., I. Doudevski, H. Lin, R. Azimova, D. Ng, B. Frangione, B. Kagan, J. Ghiso, and R. Lal, 2005. Amyloid ion channels: A common structural link for protein misfolding disease. *Proc. Natl. Acad. Sci. USA* 102:10427–10432.

31. Arispe, N., H. Pollard, and E. Rojas, 1994. β-Amyloid Ca^{2+}-channel hypothesis for neuronal death in Alzheimer disease. *Mol. Cell. Biochem.* 140:119–125.

32. Lin, H., Y. Zhu, and R. Lal, 1999. Amyloid β protein (140) forms calcium-permeable, Zn^{2+}-sensitive channel in reconstituted lipid vesicles. *Biochemistry* 38:11189–11196.

33. Rhee, S. K., A. P. Quist, and R. Lal, 1998. Amyloid β protein-(142) forms calcium-permeable, Zn^{2+}-sensitive channel. *J. Biol. Chem.* 273:13379–13382.

34. Hirakura, Y., I. Carreras, J. D. Sipe, and B. L. Kagan, 2002. Channel formation by serum amyloid A: a potential mechanism for amyloid pathogenesis and host defense. *Amyloid* 9:13–23.

35. Jang, H., J. Zheng, R. Lal, and R. Nussinov, 2008. New structures help the modeling of toxic amyloid beta ion channels. *Trends Biochem.Sci.* 33:91–100.

36. Jang, H., J. Zheng, and R. Nussinov, 2007. Models of beta-amyloid ion channels in the membrane suggest that channel formation in the bilayer is a dynamic process. *Biophys. J.* 93:1938–1949.

37. Jang, H., F. T. Arce, R. Capone, S. Ramachandran, R. Lal, and R. Nussinov, 2009. Misfolded Amyloid Ion Channels Present Mobile beta-Sheet Subunits in Contrast to Conventional Ion Channels. *Biophys. J.* 97:3029–3037.

38. Strodel, B., J. Lee, C. Whittleston, and D. Wales, 2010. Transmembrane structures for Alzheimer's Aβ_{1-42} oligomers. *J. Am. Chem. Soc.* 132:13300–13312.

39. Chang, Z., Y. Luo, Y. Zhang, and G. Wei, 2011. Interactions of Aβ25-35 -Barrel-Like Oligomers with Anionic Lipid Bilayers and Resulting Membrane Leakage: An All-Atom Molecular Dynamics Study. *J. Phys. Chem. B* 115:1165–1174.

40. Lemkul, J. A., and D. R. Bevan, 2008. A comparative molecular dynamics analysis of the amyloid beta-peptide in a lipid bilayer. *Arch. Biochem. Biophys.* 470:54–63.

41. Lemkul, J. A., and D. R. Bevan, 2009. Perturbation of membranes by the amyloid beta-peptide - a molecular dynamics study. *FEBS J.* 276:3060–3075.

42. Lemkul, J. A., and D. R. Bevan, 2011. Lipid composition influences the release of Alzheimer's amyloid -peptide from membranes. *Protein Sci.* in press.

43. Davis, C. H., and M. L. Berkowitz, 2009. Interaction Between Amyloid-b (1-42) Peptide and Phospholipid Bilayers: A Molecular Dynamics Study. *Biophysical J.* 96:785–797.

44. Davis, C. H., and M. L. Berkowitz, 2009. Structure of the Amyloid-beta (1-42) Monomer Absorbed To Model Phospholipid Bilayers: A Molecular Dynamics Study. *J. Phys. Chem. B* 113:14480–14486.

45. Davis, C. H., and M. L. Berkowitz, 2010. A molecular dynamics study of the early stages of amyloid-beta(1-42) oligomerization: The role of lipid membranes. *Proteins* 78:2533–2545.

46. Xu, Y. C., J. J. Shen, X. M. Luo, W. L. Zhu, K. X. Chen, J. P. Ma, and H. L. Jiang, 2005. Conformational transition of amyloid beta-peptide. *Proc. Natl. Acad. Sci. U. S. A.* 102:5403–5407.

47. Miyashita, N., J. E. Straub, and D. Thirumalai, 2009. Structures of β-Amyloid Peptide 1–40, 1–42, and 1–55—the 672–726 Fragment of APP—in a Membrane Environment with Implications for Interactions with γ-Secretase. *J. Am. Chem. Soc.* 131:17843–17852.

48. Friedman, R., R. Pellarin, and A. Caflisch, 2009. Amyloid aggregation on lipid bilayers and its impact on membrane permeability. *J. Mol. Biol.* 387:407–415.

49. Friedman, R., R. Pellarin, and A. Caflisch, 2010. Soluble Protofibrils as Metastable Intermediates in Simulations of Amyloid Fibril Degradation Induced by Lipid Vesicles. *J. Phys. Chem. Lett.* 1:471–474.

50. Mobley, D. L., D. L. Cox, R. R. P. Singh, M. W. Maddox, and M. L. Longo, 2004. Modeling amyloid beta-peptide insertion into lipid bilayers. *Biophys. J.* 86:3585–3597.

51. Hess, B., C. Kutzner, D. van der Spoel, and E. Lindahl, 2008. GROMACS 4: Algorithms for Highly Efficient, Load-Balanced, and Scalable Molecular Simulation. *J. Chem. Theor. Comput.* 4:435–447.

52. Oostenbrink, C., A. Villa, A. E. Mark, and W. F. V. Gunsteren, 2004. A biomolecular force field based on the free enthalpy of hydration and solvation: The GROMOS force-field parameter sets 53A5 and 53A6. *J. Comput. Chem.* 25:1656–1676.

53. Kukol, A., 2009. Lipid Models for United-Atom Molecular Dynamics Simulations of Proteins. *J. Chem. Theory Comput.* 5:615–626.

54. Kabsch, W., and C. Sander, 1983. Dictionary of protein secondary structure - pattern-recognition of hydrogen-bonded and geometrical features. *Biopolymers* 22:2577–2637.

55. Allen, W. J., J. A. Lemkul, and D. R. Bevan, 2009. GridMAT-MD: A Grid-Based Membrane Analysis Tool for Use With Molecular Dynamics. *J. Comput. Chem.* 30:1952–1958.

56. Cordomí, A., and J. J. Perez, 2007. Molecular Dynamics Simulations of Rhodopsin in Different One-Component Lipid Bilayers. *J. Phys. Chem. B* 111:7052–7063.

57. Shafrir, Y., S. Durell, N. Arispe, and H. R. Guy, 2010. Models of membrane-bound Alzheimer's Abeta peptide assemblies. *Proteins: Struct., Func. and Bioinf.* 78:3473–3487.

58. Vacha, R., M. L. Berkowitz, and P. Jungwirth, 2009. Molecular Model of a Cell Plasma Membrane With an Asymmetric Multicomponent Composition: Water Permeation and Ion Effects. *Biophys. J.* 96:4493–4501.

59. Wirths, O., G. Multhaup, and T. A. Bayer, 2004. A modified beta-amyloid hypothesis: intraneuronal accumulation of the beta-amyloid peptide–the first step of a fatal cascade. *J Neurochem.* 91:513–520.

60. Durell, S., H. Guy, N. Arsipe, E. Rojas, and H. Pollard, 1994. Theoretical models of the ion channel structure of amyloid β-protein. *Biophys. J.* 67:2137–2145.

61. Kandt, C., W. L. Ash, and D. P. Tieleman, 2007. Setting up and running molecular dynamics simulations of membrane proteins. *Methods* 41:475–488.

Table 1: Effects of Aβ_{42} on lipid bilayers in terms of area per lipid headgroup, bilayer thickness, translocation of water, and number of H-bonds between Aβ_{42} and lipids in the hydrophobic membrane core. Given are average values calculated for the last 400 ns of the 500 ns MD simulations.

Aβ_{42} structure	Bilayer	Area per lipid [Å^2]^a		Bilayer thickness [nm]^b	Water passage	number H-bonds
		Top leaflet	Bottom leaflet			
SHEET		62.6	63.4	3.55	yes	18
HEL-16	POPC	63.4	67.5	3.54	no	6
HEL-23		65.2	68.5	3.50	no	3
SHEET		53.7	54.5	4.15	yes	19
HEL-16	DPPC	50.9	56.6	4.03	no	18
HEL-23		51.8	57.1	4.16	no	2
SHEET		69.3	69.3	3.45	yes	13
HEL-16	POPG	64.0	69.7	3.43	yes	9
HEL-23		64.0	68.7	3.45	yes	9
tetramer	POPC	62.0	65.3	3.49	yes	95

^{a} The values for the areas per lipid of the pure membranes obtained from 40 ns MD simulations are 69.3 Å^2 for POPC, 62.3 Å^2 for DPPC, and 70.0 Å^2 for POPG (53).
^{b} The simulation values for the bilayer thickness of the pure bilayers are 3.51 nm for POPC, 3.71 nm for DPPC and 3.48 nm for POPG (53).

Figure Legends

Figure 1.

Initial structures for the MD runs: (a) β-sheet monomer (SHEET), (b) β-sheet tetramer, (c) α-helix inserted with K16 at the membrane-water interface (HEL-16), (d) α-helix inserted with D23 at the membrane-water interface (HEL-23). The peptide is shown in cartoon and colored based on the physicochemical properties of the residues: blue, basic; red, acidic; white, hydrophobic; green, polar. The bilayer phosphorus atoms are shown as van der Waals spheres in tan color. Lipid tails and water molecules are not shown for clarity.

Figure 2.

Final states after 500 ns MD simulations of $A\beta_{42}$ in POPC (PC), DPPC (DC) and POPG (PG) bilayers. For coloring explanation see Fig. 1. Peptide residues marked with pink spheres are involved in H-bond formation with the water molecules entering the bilayer.

Figure 3.

Final states after 500 ns MD simulations of helical $A\beta_{42}$ (HEL-23) in mixed (a) POPC/POPG and (b) POPG/POPC bilayers, where the order of the lipid type refers to the upper/lower leaflet. For coloring explanation see Fig. 2.

Figure 4.

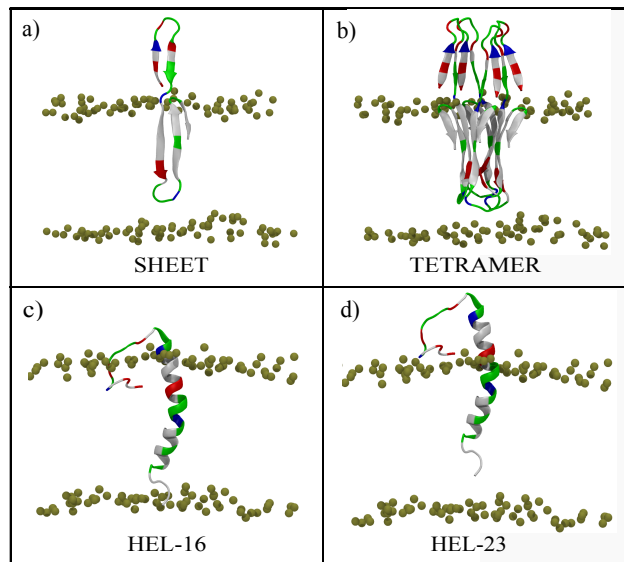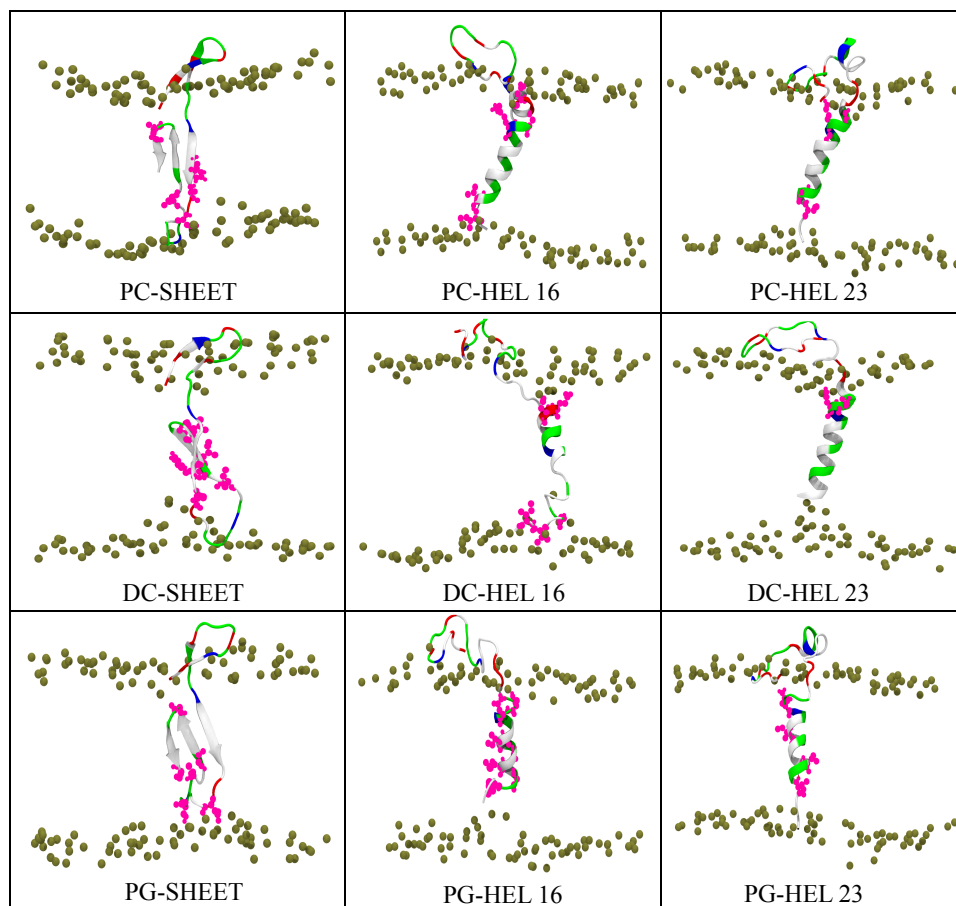Final state of the 500 ns MD simulation of the $A\beta_{42}$ β-sheet tetramer in a POPC bilayer. For coloring explanation see Fig. 2.
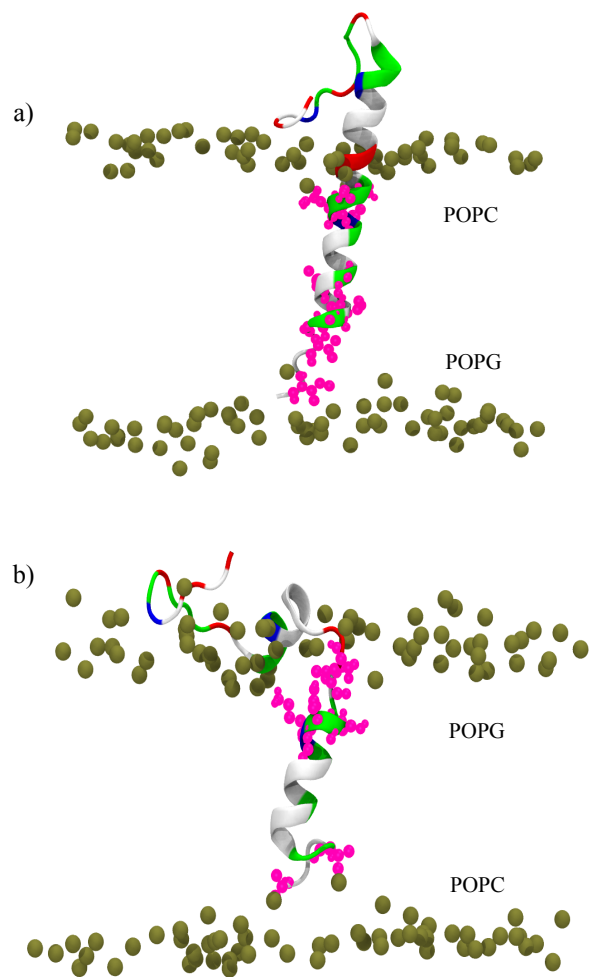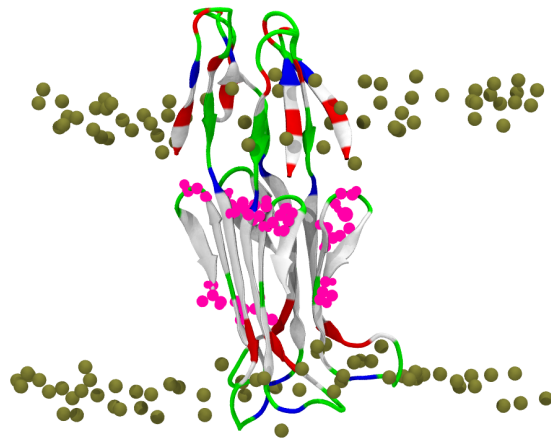
Figure 1:

Figure 2:

Figure 3:

Figure 4: